Motion of particles in Schwarzschild black hole surrounded by an external electrostatic field

A. Al-Badawi

Department of Physics, Al-Hussein Bin Talal University, P. O. Box: 20, 71111, Ma'an, Jordan

E-mail: ahmadbadawi@ahu.edu.jo

Abstract

In this paper, we discussed the motion of neutral and charged particles in Schwarzschild black hole immersed in an electromagnetic universe (SEBH). The SEBH represents a mass M coupled to an external electromagnetic field that was derived from the metric of colliding electromagnetic waves with double polarization. Our study examine how the external electromagnetic field affects the trajectory of neutral and charged particles. First, the trajectories of both photon and test particle are studied. Then, the exact solutions for the trajectories are obtained in terms of the Jacobi-elliptic integrals for all possible energy and angular momentum of test particle and photon. We have also discussed the motion of charged particle and obtained the radius of the innermost circular orbit (ISCO). It is especially interesting when the charge sign is positive since this creates a conflict between gravitational (attraction force) and electric (repulsion force). Furthermore, we discuss the Lyapunov exponent and the effective force influencing particles in SEBH spacetime.

Keywords: Schwarzschild; external electrostatic field; particle motion; Jacobi-elliptic integrals; Lyapunov exponent; effective force.

I. INTRODUCTION

A solution to the Einstein-Maxwell field equations describing a mass M coupled to an external electromagnetic (EM) field has been found in [1-2]. This solution namely, Schwarzschild (S) black hole (BH) immersed in an EM universe or Schwarzschild-Electromagnetic black hole (SEBH) is originated from the metric of colliding EM waves with double polarization [3]. There are two physical parameters in the SEBH spacetime, the gravitational mass and the interpolation parameter, which interpolate two well-known solutions to General Relativity, SBH and Bertotti-Robinson solution [4, 5]. The EM field in SEBH spacetime originates from the already-existing EM radiation, in contrast to the EM

 doi:10.20944/preprints202306.0087.v1

field in Reissner-Nordstmrö spacetime, which is created from the charged black hole.

On the other hand, geodesics of BHs are studied extensively in the literature. The first study of motion of test particles was in SBH spacetime [6]. Later, the motion of test particles was examined in Reissner-Nordström spacetime [7]. Solution of the equations of motion of electrically and magnetically charged particles in terms of Weierstrass elliptic functions, in Reissner-Nordström spacetime was given in [8]. The circular orbits in Kerr spacetime has also been studied [9-10]. The solution to timelike geodesics in terms of Weierstrass elliptic functions in Taub-NUT spacetime was studied by Kagramanova et al [11]. The charged particle motion in Kerr-Newman spacetime was analyzed in [12]. In addition to the above studies, several papers about geodesic motion in various spacetime backgrounds have been published [13-26]. The case of orbits around a BH immersed in an external electric field has unfortunately received less attention than its magnetic counterpart. For example, geodesics work has focused on the magnetic case [27-31]. The motion of charged particles in BH immersed in magnetic field was studied in [32-35]. However, the geodesics structure of SEBH has been studied in [36]. The study shows that all orbits in radial geodesics are stable and particles that fall toward the horizon in a finite proper time take longer time than the SBH. It is also shows that there are no stable circular orbits for photons in circular geodesics, as well as the exact expression for the innermost circular orbit (ISCO) for a particle in timelike geodesics was obtained. A semi-classical tunneling method is used to investigate the effect of generalized uncertainty principle on the tunneling of entangled scalars/fermions from a SEBH [37]. Whereas, the quasinormal modes of the SEBH is studied in [38].

In the present paper, we first investigate the motion of neutral and charged particles in the background of SEBH. Secondly, we examined the effects of the external EM field through the interpolation parameter on neutral and charged particle trajectories. To achieve our objectives we will obtain exact solutions for the paths of massless and massive particles in terms of the Jacobi-elliptic integrals. In addition, we will study the circular motion of a test particle with a charge per unit mass and determine the radius of the innermost circular orbit (ISCO). Our analysis of the motion of a charged particle reveals an interesting result: if the charge sign is positive, it shows an unphysical behavior due to the clash between the attractive gravitational force of the BH and the repulsive electric force of the external EM field. Further, we study the Lyapunov exponent and the effective force acting on the particles in background of SEBH.

Preprints (www.preprints.org) | NOT PEER-REVIEWED | Posted: 1 June 2023 doi:10.20944/preprints202306.0087.v1

The motivation of test particle studies, both charged and uncharged, is one way to understand the gravitational field around a BH. Because the motion of test particles around BHs is determined by the geodesics structure, it is important to analyze the geodesics structure carefully. All phenomena such as light deflection, perihelion shift, Lense-Thirring effect and gravitational time-delay etc. are related to the motion of particles around BHs. Moreover, investigating the orbits of particles is of astrophysical relevant when studying the flow of particles in accretion disks around BHs. In recent years, test particles motion near BHs or naked singularities has became an interesting subject, while the dynamics motion of charged particles in Reissner-Nordström spacetime has revealed that BHs and naked singularities can be distinguished [39-41]. Test particles moving along circular orbits are particularly appropriate to measure the effects generated by naked singularities [42]. Therefore, the purpose of the current paper is to study once again the motion of test particles (neutral and charged) in the presence of a BH immersed in an external EM field.

This paper is organized as follows: in Sect. 2, SEBH spacetime is introduced and geodesic equations are derived. Sections 3 and 4 present analytical solutions of null and timelike geodesics, respectively. In Sect. 5, we discuss the motion of massive charged particles in SEBH spacetime. The force acting on the particle and the Lyapunov exponent are studied in Sect. 6. Finally, Our conclusion will be presented in Sect. 7.

II. SEBH SPACETIME AND GEODESIC EQUATIONS

The SEBH solution [1-2] is given by

$$ds^2 = -f(r)\,dt^2 + \frac{dr^2}{f(r)} + r^2\left(d\theta^2 + \sin^2\theta d\phi^2\right), \tag{1}$$

where

$$f(r) = 1 - \frac{2M}{r} + \frac{M^2}{r^2}\left(1 - a^2\right), \tag{2}$$

in which, M is the BH mass coupled to an external EM field and $a\,(0 < a \leq 1)$ is the interpolation parameter [3, 37]. This metric meets all the required limits as boundary conditions, when $a = 1$ we get SBH metric and for $0 < a \leq 1$ we get SEBH. This case $(a = 0)$, which is excluded, is the extremal Reissner-Nordström that is transformable to

Preprints (www.preprints.org) | NOT PEER-REVIEWED | Posted: 1 June 2023 doi:10.20944/preprints202306.0087.v1

Bertotti-Robinson metric. There are two horizons in the metric (1)

$$r_{in} = M(1-a). \tag{3}$$

$$r_{out} = M(1+a) \tag{4}$$

The outer horizon r_{out} is similar to the event horizon $r = 2M$ of SBH while the inner horizon r_{in} is a cosmological horizon. Figure 1 depicts the variation of function $f(r)$ with the parameter a to illustrate the effect of the interpolation parameter in SEBH spacetime. It is obvious that as a increases its value, the separation distance between the two horizons gets farther. Furthermore, to clarify the effect of the interpolation parameter a, we compute

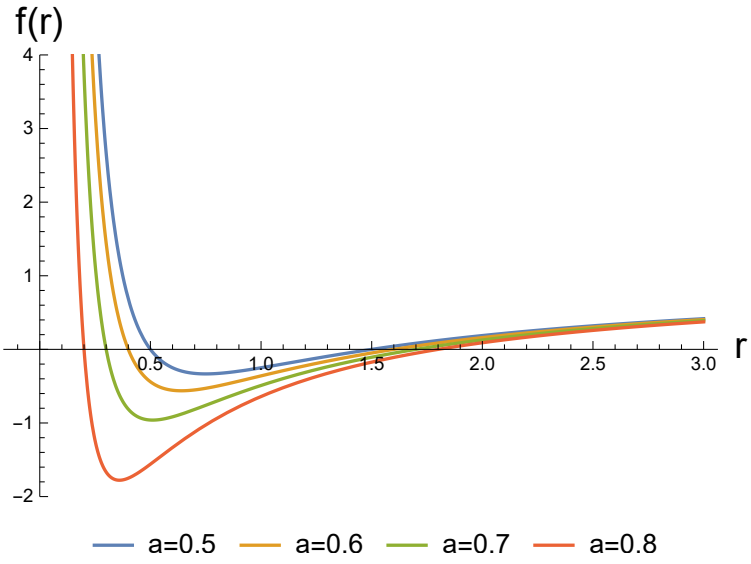

FIG. 1: The variation of function $f(r)$ with interpolation parameter a. Here $M = 1$.

the Weyl and Ricci scalars using the Newman-Penrose formalism [43]. We choose the null tetrad 1-form $(l, n, m, \overline{m})$ which satisfies the orthogonality conditions $(l.n = -m.\overline{m} = 1)$, as

$$l_\mu = dt - \frac{dr}{f(r)},$$

$$2n_\mu = f(r)\,dt + dr,$$

$$m_\mu = \frac{-r}{\sqrt{2}}(d\theta + i\sin\theta d\phi),$$

$$\overline{m}_\mu = \frac{-r}{\sqrt{2}}(d\theta - i\sin\theta d\phi). \tag{5}$$

Preprints (www.preprints.org) | NOT PEER-REVIEWED | Posted: 1 June 2023 doi:10.20944/preprints202306.0087.v1

Thus, the non-zero Weyl and Ricci scalars can be obtained as follows

$$\Psi_2 = \frac{-M}{r^4}\left[r - M\left(1-a^2\right)\right] \tag{6}$$

$$\Phi_{11} = \frac{M^2\left(1-a^2\right)}{2r^4}, \tag{7}$$

Consequently, our metric (1) belongs to Petrov type-D spacetimes and it satisfies all the required limits as boundary conditions

$$(a=1) \rightarrow \left(\Psi_2 = \frac{-M}{r^3}, \Phi_{11} = 0\right) \rightarrow (Gravity)$$

$$(0<a<1) \rightarrow \left(\Psi_2 \neq 0 \neq \Phi_{11}\right) \rightarrow (Gravity + EM).$$

Hence, the effect of parameter a is clear.

Our next step will be to derive the geodesic equations for neutral particles around the SEBH using the same approach presented in Chandrasekhar's well-known book [10]. The equations governing the geodesics in the background geometry (1) can be derived from the Lagrangian,

$$L = \frac{1}{2}\left[-f\left(r\right)\dot{t}^2 + \frac{\dot{r}^2}{f\left(r\right)} + r^2\left(\dot{\theta}^2 + \sin^2\theta\dot{\phi}^2\right)\right], \tag{8}$$

in which a dot denotes a differentiation with respect to an affine parameter s along the geodesics. Because the SEBH spacetime (1) has two Killing vectors, there are two constants of motion which can be labeled as E and ℓ, therefore

$$E = -f\left(r\right)\dot{t}, \tag{9}$$

and

$$\ell = r^2\sin^2\theta\dot{\phi}. \tag{10}$$

We will consider the motion restricted to the equatorial plane with $\theta = \pi/2$ and $\dot{\theta} = 0$. With two constants of motion given in Eqs. (9) and (10) the geodesics equation becomes

$$\left(\frac{dr}{d\phi}\right)^2 = \frac{r^4}{\ell^2}\left(E^2 - \left(1 - \frac{2M}{r} + \frac{M^2}{r^2}\left(1-a^2\right)\right)\right)\left(\epsilon + \frac{\ell^2}{r^2}\right). \tag{11}$$

We can obtain the r equations as a function of s and t as follows

$$\left(\frac{dr}{ds}\right)^2 + 2V_{eff}\left(r\right) = E^2, \tag{12}$$

$$\left(\frac{dr}{dt}\right)^2 = \left(1 - \frac{2}{E^2}V_{eff}\left(r\right)\right)\left(1 - \frac{2M}{r} + \frac{M^2}{r^2}\left(1-a^2\right)\right)^2. \tag{13}$$

Preprints (www.preprints.org) | NOT PEER-REVIEWED | Posted: 1 June 2023 doi:10.20944/preprints202306.0087.v1

where the effective potential $V_{eff}(r)$ can be defined as

$$V_{eff}(r) = \frac{1}{2}\left(1 - \frac{2M}{r} + \frac{M^2}{r^2}\left(1 - a^2\right)\right)\left(\epsilon + \frac{\ell^2}{r^2}\right). \tag{14}$$

To study the orbits, we consider r as a function of ϕ and replacing r by $u = 1/r$ as the independent variable, hence we obtain the equation

$$\left(\frac{du}{d\phi}\right)^2 = \frac{E^2}{\ell^2} - \left(1 - 2Mu + M^2\left(1 - a^2\right)u^2\right)\left(\frac{\epsilon}{\ell^2} + u^2\right) = g(u). \tag{15}$$

We choose $(\epsilon = 0)$ for null and $(\epsilon = 1)$ for timelike geodesic.

III. THE NULL GEODESICS OF SEBH ($\epsilon = 0$)

Here, we shall study the motion of the radial geodesics in zero angular momentum which means that particle will move radially. The equations that governing the null geodesics are

$$\frac{dr}{ds} = \pm E, \tag{16}$$

$$\frac{dr}{dt} = \pm\left(1 - \frac{2M}{r} + \frac{M^2}{r^2}\left(1 - a^2\right)\right), \tag{17}$$

$$\left(\frac{du}{d\phi}\right)^2 = -M^2\left(1 - a^2\right)u^4 + 2Mu^3 - u^2 + \frac{1}{D^2} = g(u). \tag{18}$$

where $D = \frac{\ell}{E}$ is the impact factor. The radial equations (16) and (17) which corresponds to zero angular momentum (i.e. $\ell = 0$) are solved exactly in Ref. [36]. However, we are interested in Eq. (18) which describes the structure of the geodesics. This structure will depend on the roots of the function $g(u)$. Here, for $u \to \mp\infty$, $g(u) \to -\infty$. Also when $u \to 0, g(u) \to \frac{1}{D^2}$. Therefore $g(u)$ has two real roots, one negative and one positive. The other two possible roots could be two more real roots, complex conjugate pair or $g(u)$ may has a degenerate root. All these possibilities are shown in Fig. 2. The root structure of $g(u)$ varies depending on the values of E, M, ℓ and a. In the following, we will discuss all types of possible orbits.

Case I) The equation $g(u) = 0$ has four real and distinct roots as shown in Fig. 2a. Note that it is possible in case of four real roots that three of them would be negative. However, according to Fig. 2a there exist two distinguished orbits limited to the intervals $0 < u < u_2$ (first kind) and $u_3 < u < u_4$ (second kind). Hence, Eq. (18) can be cast in the form

$$\frac{du}{d\phi} = \mp\sqrt{g(u)}, \tag{19}$$

Preprints (www.preprints.org) | NOT PEER-REVIEWED | Posted: 1 June 2023 doi:10.20944/preprints202306.0087.v1

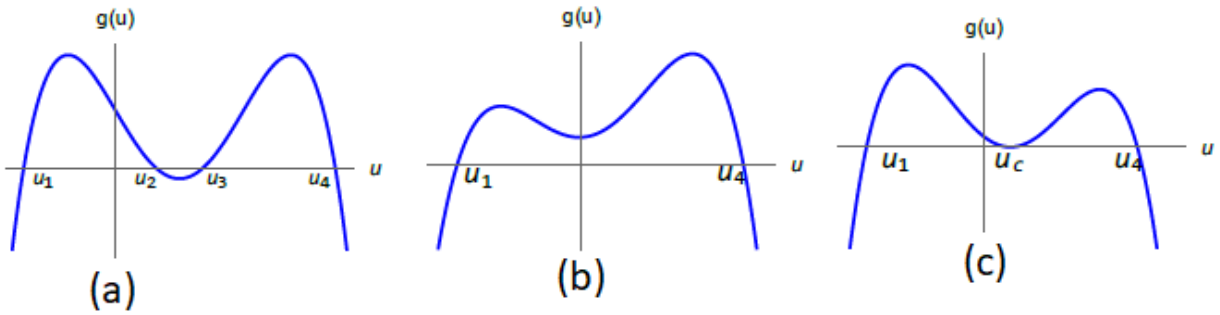

FIG. 2: The function $g(u)$ versus u. The graph shows all possible roots of the function $g(u)$.

in which $g(u)$ is written as,

$$g(u) = -M^2\left(1-a^2\right)(u-u_4)(u-u_3)(u-u_2)(u-u_1) \ . \tag{20}$$

We will choose the "+" sign without loss of generality. To get the first kind orbits, we integrate Eq. (19) and obtain a relation between u and ϕ in terms of Jacobi-elliptic integral $\mathcal{F}(x,y)$,

$$\phi = \frac{2\mathcal{F}(x,y)}{M\sqrt{\left(1-a^2\right)(u_1-u_3)(u_2-u_4)}} + const, \tag{21}$$

where

$$\sin x = \sqrt{\frac{(u_1-u)(u_2-u_4)}{(u-u_4)(u_1-u_2)}}, \tag{22}$$

$$y = \frac{(u_1-u_2)(u_3-u_4)}{(u_2-u_4)(u_1-u_3)}, \tag{23}$$

$$\mathcal{F}(x,y) = \int_0^x \frac{d\lambda}{\sqrt{1-y\sin^2\lambda}}. \tag{24}$$

Note that the above solution is also valid for second kind orbits ($u_3 < u < u_4$) with the only difference in the value of Eq. (22) as follows

$$\sin x = \sqrt{\frac{(u_3-u)(u_2-u_4)}{(u_2-u)(u_3-u_4)}}. \tag{25}$$

The corresponding orbits for first and second kind are depicted in Fig. 3.

Case II) The equation $g(u) = 0$ has a pair of complex-conjugate roots, besides two real roots as shown in Fig. 2b. Here, we have geodesic of first kind orbits with critical impact parameter. The conditions of the occurrence of double root are $g(u) = 0$, and $g'(u) = 0$. Hence,

$$g(u) = \frac{1}{D^2} - u_c^2\left(1 - 2Mu_c + M^2\left(1-a^2\right)u_c^2\right) = 0, \tag{26}$$

Preprints (www.preprints.org) | NOT PEER-REVIEWED | Posted: 1 June 2023 doi:10.20944/preprints202306.0087.v1

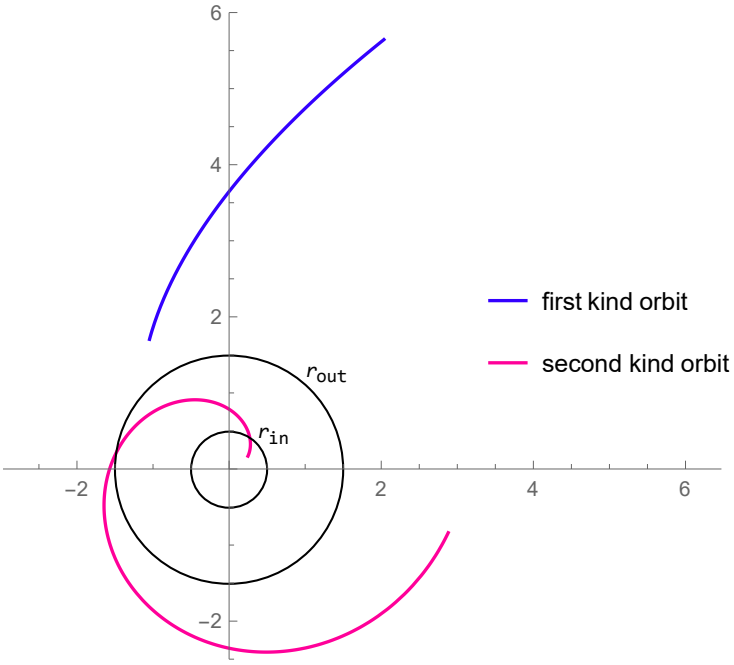

FIG. 3: The polar plot shows the null geodesics of first and second kind orbits. The first kind starts from infinity and approaches the black hole. The second kind starts above r_{out} and ends below r_{in}. Here, M = 1 and a = 0.5.

and

$$g'(u) = 2u_c\left(1 - 3Mu + 2M^2\left(1 - a^2\right)u^2\right) = 0. \tag{27}$$

It follows from Eq. (27) that the minimum radius for circular orbits u_c is given by [31]

$$u_c = \frac{3 - \sqrt{1 + 8a^2}}{4M\left(1 - a^2\right)}. \tag{28}$$

The corresponding value of r_c is

$$r_c = \frac{M}{2}(3 + \sqrt{1 + 8a^2}). \tag{29}$$

The impact parameter that corresponds to r_c is $D_c^2 = r_c^4/\left(r_c^2 - 2Mr_c + M^2\left(1 - a^2\right)\right)$. When $D = D_c$, then $g(u)$ can be rewritten as

$$g(u) = (u - u_c)^2\left[M\left(a^2 - 1\right)u^2 + \left(2 - 2M\left(1 - a^2\right)u_c\right)u + u_c - M\left(1 - a^2\right)u_c^2\right]M. \tag{30}$$

Thus, to obtain the solution for ϕ we have to solve

$$\phi = \pm\int \frac{du}{\sqrt{(u - u_c)^2\left[M\left(a^2 - 1\right)u^2 + \left(2 - 2M\left(1 - a^2\right)u_c\right)u + u_c - M\left(1 - a^2\right)u_c^2\right]M}}, \tag{31}$$

Preprints (www.preprints.org) | NOT PEER-REVIEWED | Posted: 1 June 2023 doi:10.20944/preprints202306.0087.v1

and the solution is given by

$$\phi = \pm\frac{1}{A}\ln\left(2A\xi + B + 2A\sqrt{A\left(M^2\left(a^2-1\right)+B\xi+A\xi^2\right)}\right), \tag{32}$$

where

$$A = \frac{3\sqrt{1+8a^2}-\left(1+8a^2\right)}{4\left(1-a^2\right)}, \tag{33}$$

$$B = M\sqrt{1+8a^2}-M, \tag{34}$$

and

$$\xi = \frac{1}{u-u_c}. \tag{35}$$

An example to circular orbits is shown in Fig. 4.

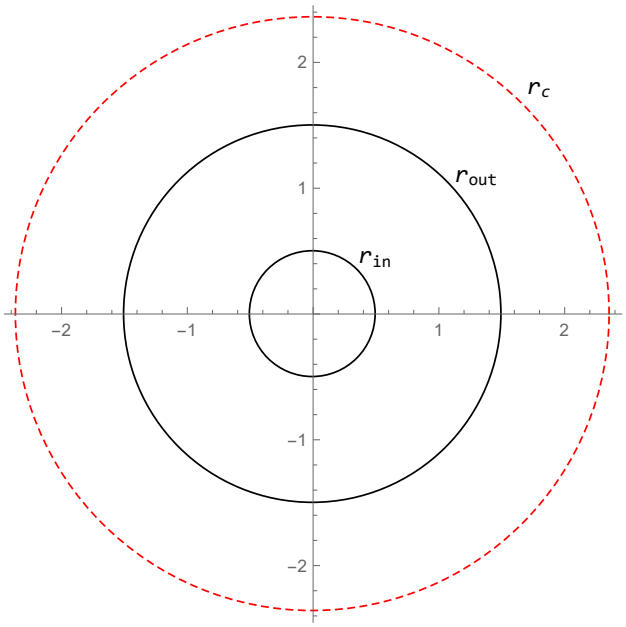

FIG. 4: The graph shows null geodesics representing by the unstable circular orbit when a = 0.5 and M = 1, we get $r_c = 2.36, r_{in} = 0.5$ and $r_{out} = 1.5$.

Case III) The equation $g(u) = 0$ has a double root (see Fig. 2c). Then, we have orbits with imaginary eccentricity. Hence, $g(u)$ can be rewritten as

$$g\left(u\right) = -M^2\left(1-a^2\right)\left(u-u_4\right)\left(u-u_2\right)\left(u-\overline{u}_2\right)\left(u-u_1\right), \tag{36}$$

and solution is given by

$$\phi = \frac{\mathcal{F}(x,y)}{M\sqrt{\left(1-a^2\right)NB}} + const, \tag{37}$$

Preprints (www.preprints.org) | NOT PEER-REVIEWED | Posted: 1 June 2023 doi:10.20944/preprints202306.0087.v1

where

$$\cos x = \frac{(u_4 - u)\, B - (u - u_1)\, N}{(u_4 - u)\, B + (u - u_1)\, N}, \tag{38}$$

$$y^2 = \frac{(u_1 - u_4)^2 - (N - B)^2}{4NB}, \tag{39}$$

$$N = \frac{1}{2}\sqrt{(2u_4 - u_2 - \overline{u}_2)^2 + (u_2 - \overline{u}_2)^2}, \tag{40}$$

$$B = \frac{1}{2}\sqrt{(2u_1 - u_2 - \overline{u}_2)^2 - (u_2 - \overline{u}_2)^2}, \tag{41}$$

$$\mathcal{F}(x, y) = \int_0^x \frac{d\lambda}{\sqrt{1 - y \sin^2 \lambda}}. \tag{42}$$

The corresponding orbit with imaginary eccentricity is shown in Fig. 5.

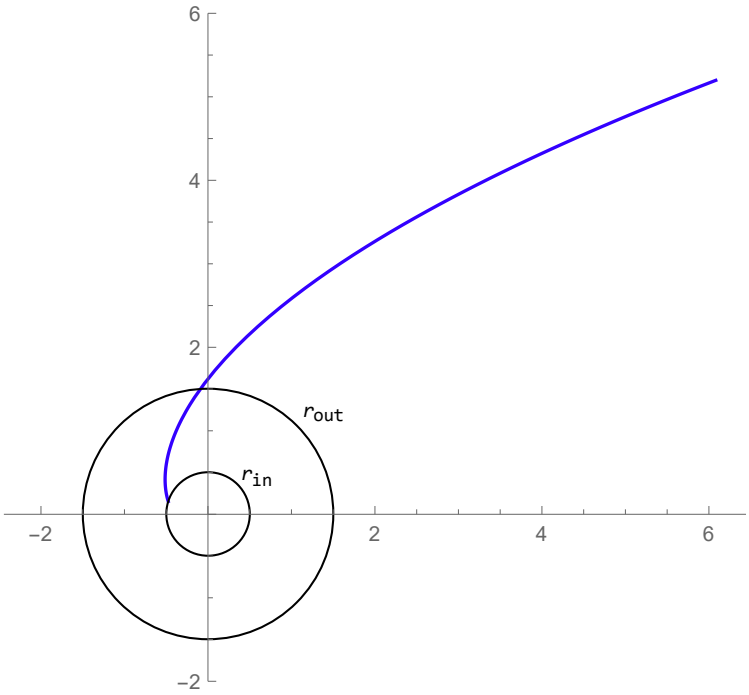

FIG. 5: The polar plot shows null geodesics with imaginary eccentricity. The trajectory starts in infinity and ends below r_{out}. Here, M = 1 and a = 0.5.

IV. TIMELIKE GEODESICS OF SEBH($\epsilon = 1$)

In this section, we will study the orbits for massive particles. Hence, the trajectory equation that governing the timelike geodesics is

$$\left(\frac{du}{d\phi}\right)^2 = -M^2\left(1 - a^2\right)u^4 + 2Mu^3 - \left(1 + \frac{M^2\left(1 - a^2\right)}{\ell^2}\right)u^2 + \frac{2M}{\ell^2}u + \frac{E^2 - 1}{\ell^2} = g\left(u\right), \tag{43}$$

Preprints (www.preprints.org) | NOT PEER-REVIEWED | Posted: 1 June 2023 doi:10.20944/preprints202306.0087.v1

and the effective potential is given by

$$V_{eff}(r) = \frac{1}{2}\left(1 - \frac{2M}{r} + \frac{M^2}{r^2}\left(1 - a^2\right)\right)\left(1 + \frac{\ell^2}{r^2}\right). \tag{44}$$

Since $\left(\frac{dr}{ds}\right)^2 + 2V_{eff}(r) = E^2$, the geometry of the orbits described by Eq.(43) depends on the values of E. To display the energy levels we make a plot of the effective potential (44) in Fig. 6 where the energy levels E_1, E_c and E_2 are specified. Those energy levels correspond

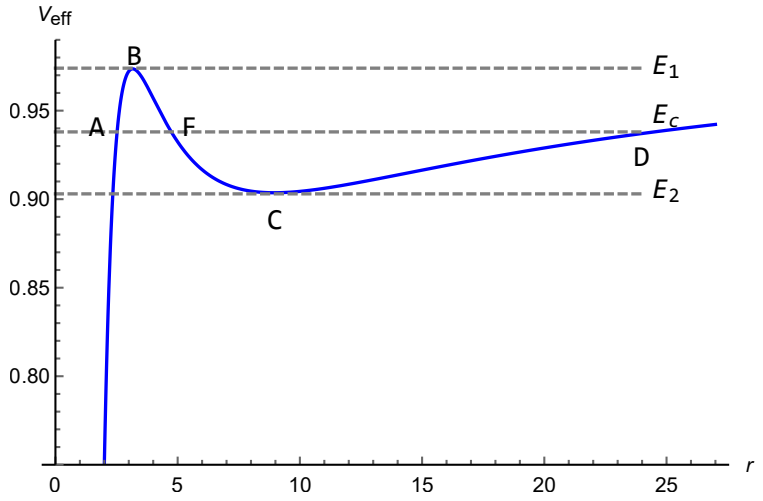

FIG. 6: The effective potential V_{eff} for massive particles versus r. The graph shows the relation of V_{eff} with the energy E (M = 1, a = 0.5 and $\ell^2 = 12$).

to different scenarios of motion of the particles, we will discuss them as follow:

I) $E = E_c$: this case leads to a stable circular orbit at point C of Fig. 6. The conditions for the circular orbits are $g(u) = 0$ and $g'(u) = 0$ hence, we obtain the expressions for the energy E and the angular momentum ℓ[1] of the particle [36]

$$E^2 = \frac{\left(1 - 2Mu_c + M^2u_c^2\left(1 - a^2\right)\right)^2}{T}, \tag{45}$$

$$\ell^2 = \frac{M - M^2u_c\left(1 - a^2\right)}{u_cT} \tag{46}$$

where $u_c = 1/r_c$ is the circular orbit of the particle and $T = 1 - 3Mu_c + 2M^2u_c^2\left(1 - a^2\right)$. For a physical acceptable motion, two constraints arise naturally from Eqs. (45) and (46) namely

$$1 - 3Mu_c + 2M^2u_c^2\left(1 - a^2\right) > 0, \text{ and } \frac{1}{M\left(1 - a^2\right)} < u_c. \tag{47}$$

[1] The erroneous term in ℓ^2 of Eqs. (43) and (53) of reference [36] is corrected here

Preprints (www.preprints.org) | NOT PEER-REVIEWED | Posted: 1 June 2023 doi:10.20944/preprints202306.0087.v1

From Eq.(47) the minimum radius for timelike circular orbit is same as the null circular motion given in Eq. (29). The above values of energy E and the angular momentum ℓ are suitable for a circular orbit hence, the solution of ϕ is obtained by solving the following:

$$\phi = \int \frac{\pm du}{(u-u_c)\sqrt{M\left[M\left(a^2-1\right)u^2+2\left(1-M\left(1-a^2\right)u_c\right)u+u_c\left(1-M\left(1-a^2\right)u_c-\frac{1}{u_c^2\ell^2}\right)\right]}}. \tag{48}$$

We note that the solution of Eq. (48) is same as the solution of the circular null motion (32) with minor change namely,

$$A = \frac{3\sqrt{1+8a^2}-\left(1+8a^2\right)}{4\left(1-a^2\right)} - \left(\frac{3-\sqrt{1+8a^2}}{4\ell\left(1-a^2\right)}\right)^2.$$

II) $E = E_1$: At this energy value, the radius $r = r_B$ is the radius of the circular orbit that is unstable. Orbits with $r >$ innermost stable circular orbits (r_{ISCO}) are stable. However, in the region $r_c < r < r_{ISCO}$ circular motion is completely unstable. This result can be corroborated by analyzing the behavior of energy (45) and angular momentum (46) of test particles. As the limiting radius $r = r_c$ is approached both Eqs. (45) and (46) diverge, indicating that an infinite amount of energy and angular momentum is necessary to reach $r = r_c$. Therefore, in this case we have unstable circular orbits at point B (Fig. 6) and the particles start from point B and then go either to point D or to the singularity. For the minimum unstable orbit the three conditions $g(u) = 0, g'(u) = 0$ and $g''(u) = 0$ must satisfied hence,

$$g''(u) = 6M^2\left(1-a^2\right)u^2 - 6Mu + 1 + \frac{M^2\left(1-a^2\right)}{\ell^2} = 0 \tag{49}$$

Using Eq. (46) we can eliminate ℓ^2 from Eq. (49) which can be rewrite as follows

$$4M^3\left(1-a^2\right)^2 u_c^3 - 9M^2\left(1-a^2\right)u_c^2 + 6Mu_c - 1 = 0, \tag{50}$$

Consequently Eq. (43) becomes

$$\left(\frac{du}{d\phi}\right)^2 = M\left(u-u_c\right)^3\left[2-3M\left(1-a^2\right)u_c - M\left(1-a^2\right)u\right], \tag{51}$$

thus, the solution of Eq. (51) is

$$u - u_c = \frac{2}{M}\left[\frac{1-2M\left(1-a^2\right)u_c}{\left(1-2M\left(1-a^2\right)u_c\right)^2\left(\phi-\phi_0\right)^2+\left(1-a^2\right)}\right]. \tag{52}$$

Preprints (www.preprints.org) | NOT PEER-REVIEWED | Posted: 1 June 2023 doi:10.20944/preprints202306.0087.v1

III) $E = E_2$: In this case we have first and second kind orbits. The first kind bound orbits are between points D and F (shown in Fig. 6) where particles precess around the BH. The solution of first kind bound orbits is identical to the case of first kind orbits of null geodesics given in Eq. (21). Whereas the case of the unbound second kind orbit (at point A in Fig. 6), the particles start above the outer horizon and fall into the singularity.

IV) $E > E_1$: In this case there exists unbound orbits for particles crossing point D (see Fig. 6). Hence there are possible fly-by orbits.

V. THE MOTION OF A CHARGED PARTICLE IN SEBH

In this section we will study the circular motion of a test particle which has a charge per unit mass q, in the presence of a BH coupled to an external EM field. Recall that the SEBH has an electric scalar potential of the form $\sim \frac{+M\sqrt{1-a^2}}{ar}$ [37] hence, the Lagrangian

$$2L = -f(r)\,\dot{t}^2 + \frac{1}{f(r)}\dot{r}^2 + r^2\left(\dot{\theta}^2 + \sin^2\theta\dot{\phi}^2\right) + \frac{qM\sqrt{1-a^2}}{ar}\dot{t}. \tag{53}$$

The trajectory equation for the charged particle is,

$$\left(\frac{du}{d\phi}\right)^2 = -M^2\left(1-a^2\right)u^4 + 2Mu^3 - \left(\frac{a^2\ell^2 + M^2\left(1-a^2\right)\left(a^2-q^2\right)}{a^2\ell^2}\right)u^2$$
$$+ \frac{2M}{a\ell^2}\left(a - qE\sqrt{1-a^2}\right)u + \frac{E^2-1}{\ell^2} = g(u) \tag{54}$$

The conditions for the occurrence of circular orbits are $g(u) = 0$ and

$$g'(u) = -4M^2\left(1-a^2\right)u^3 + 6Mu^2 - 2\left(\frac{a^2\ell^2 + M^2\left(1-a^2\right)\left(a^2-q^2\right)}{a^2\ell^2}\right)u$$
$$+ \frac{2M}{a\ell^2}\left(a - qE\sqrt{1-a^2}\right) = 0 \tag{55}$$

The expressions for energy E and angular momentum ℓ of the circular orbit of radius $r_c = 1/u_c$ can be obtained from the above two conditions hence,

$$E^2 = \frac{\left(1-2Mu_c + M^2\left(1-a^2\right)u_c^2\right)^2}{T} + \frac{qME\sqrt{1-a^2}\left[1-4Mu_c + 3M^2\left(1-a^2\right)u_c^2\right]u_c}{aT}$$
$$+ \frac{q^2M^3\left(1-a^2\right)\left[1-M\left(1-a^2\right)u_c\right]u_c^3}{a^2T} \tag{56}$$

$$\ell^2 = \frac{M - M^2\left(1-a^2\right)u_c - \frac{q}{a^2}\sqrt{1-a^2}\left(aE - qM^2\sqrt{1-a^2}u_c\right)}{Tu_c}. \tag{57}$$

Preprints (www.preprints.org) | NOT PEER-REVIEWED | Posted: 1 June 2023 doi:10.20944/preprints202306.0087.v1

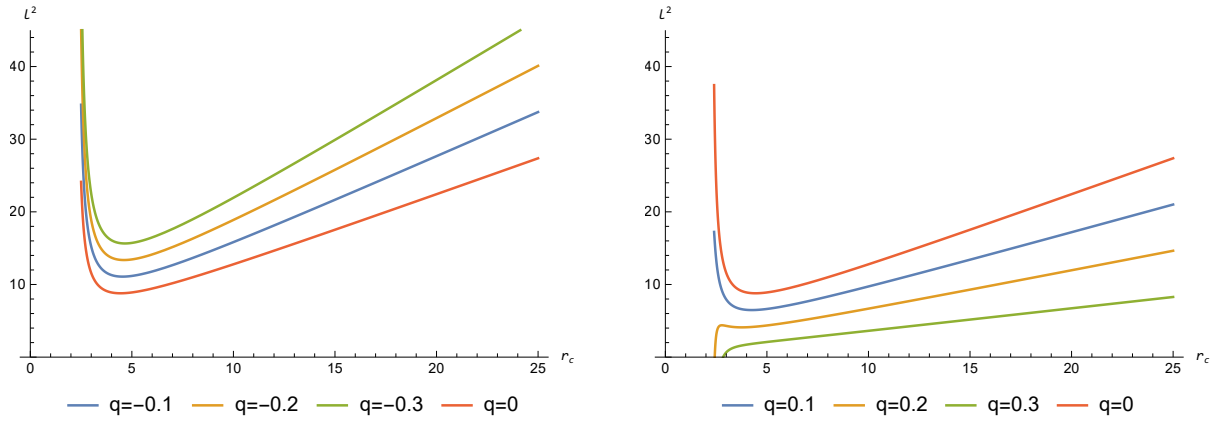

FIG. 7: Angular momentum behavior of a charged particle versus distance and different values of q. The curves of charged particles are always above the neutral particle when q is negative (left) and below when q is positive (right). ($M = 1$ and $a = 0.5$).

Having the value q in Eqs. (56) and (57) indicates that the electric force is non-geometric force and a charged particle does not follow a geodesic trajectory. The expressions of E^2 and ℓ^2 can be written explicitly up to order $(1 - a^2)$ as follows

$$E^2 = \frac{\left(1 - 2Mu_c + M^2\left(1 - a^2\right)u_c^2\right)^2}{T} +$$
$$qMu_c\sqrt{1 - a^2}\frac{\left(1 - 4Mu_c + 3M^2\left(1 - a^2\right)u_c^2\right)\left(1 - 2Mu_c + M^2\left(1 - a^2\right)u_c^2\right)}{aT^{3/2}}, \tag{58}$$

$$\ell^2 = \frac{M - M^2\left(1 - a^2\right)u_c}{Tu_c} - q\frac{\sqrt{1 - a^2}\left(1 - 2Mu_c + M^2\left(1 - a^2\right)u_c^2\right)}{T^{3/2}u_c}. \tag{59}$$

To exam the influence of the sign of the charged particle on the angular momentum ℓ^2 the Eq. (59) is displayed in Fig. 7. The figure shows the variation of ℓ^2 versus r_c for fixed values of a, M and different values of q. We can argue that in the case of a negative sign the effect of the charged particle is not notable, since both forces (electric and the gravitational) are attractive. As a result, the behavior of the charged particle is similar to the neutral particle case as shown in Fig. 7a.

On the contrary, if the charge is positive, this impose an upper limit of the value of charge q. Furthermore, the electric force is repulsive, resulting in a clash with the attractive gravitational force. As shown in Fig. 7b, the interaction of the forces results in an unphysical behavior of the charged particle. The same behavior is seen for the E^2 versus r_c for fixed values of a, M and as well as for different values of q as shown in Fig. 8a, b. Recall that,

Preprints (www.preprints.org) | NOT PEER-REVIEWED | Posted: 1 June 2023 doi:10.20944/preprints202306.0087.v1

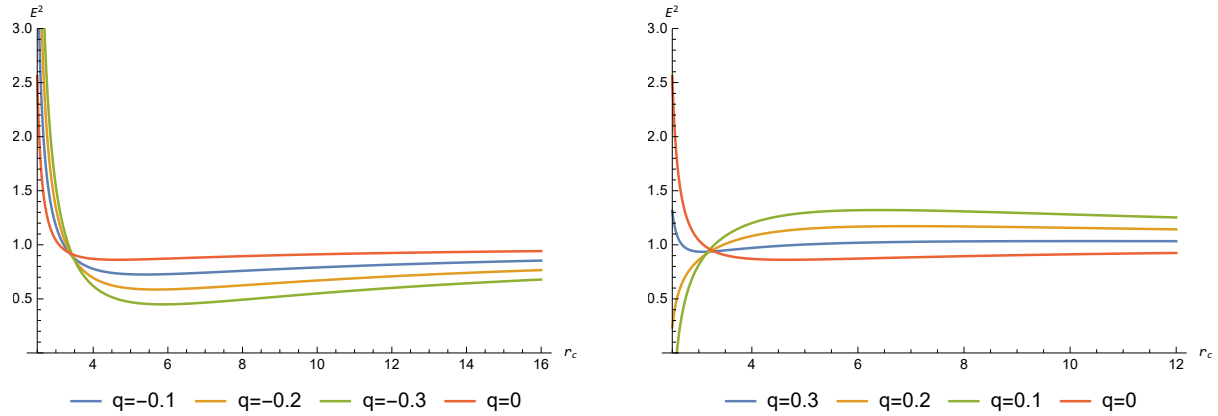

FIG. 8: Energy behavior of a massive particle versus distance and different values of q. (a) for negative values of q and (b) for positive values ($M = 1$ and $a = 0.5$).

the minimum radius for a stable circular orbit occurs at the turning point of the function $g(u)$, hence

$$g''(u) = 6M^2\left(1-a^2\right)u^2 - 6Mu + \frac{a^2\ell^2 + M^2\left(1-a^2\right)\left(a^2-q^2\right)}{a^2\ell^2} = 0 \tag{60}$$

Using Eq. (59) to eliminate ℓ^2 from Eq. (60) we get

$$4M^3\left(1-a^2\right)^2\left(\frac{q^2}{a^2}-1\right)u_c^3 + 3M^2\left(1-a^2\right)\left[3 - \frac{2qE}{a}\sqrt{1-a^2} - \frac{q^2}{a^2}\right]u_c^2 -$$

$$6M\left(1 - \frac{qE}{a}\sqrt{1-a^2}\right)u_c + 1 - \frac{qE\sqrt{\left(1-a^2\right)}}{a} = 0 \tag{61}$$

or in terms of r_c

$$r_c^3 - 6Mr_c^2 + 3M^2\left(1-a^2\right)\frac{\left[3a^2 - 2aqE\sqrt{1-a^2} + q^2\right]}{a^2 - qaE\sqrt{1-a^2}}r_c - \frac{4M^3a\left(1-a^2\right)^2\left(1-q^2\right)}{a - qE\sqrt{1-a^2}} = 0 \tag{62}$$

Ignoring terms of order $\left(1-a^2\right)^2$we obtain

$$r_c = 3M \pm 3M\sqrt{1 - \frac{\left(1-a^2\right)\left(3a^2 - 2aqE\sqrt{1-a^2} - 9q^2\right)}{3a\left(a - qE\sqrt{1-a^2}\right)}} \tag{63}$$

For neutral particle ($q = 0$,) Eq. (63) is reduced to $r_c = 3M + 3aM$ and when $a = 1$ we recover the Schwarzschild value of $r_c = 6M$. In Fig.9, we show the graphs of circular orbits for charged (63) and neutral (29) particles. In the charged particle case Fig. 9a, the circular orbit decreases as the parameter a increases in contrast to the neutral case Fig. 9b. We also observe that the circular orbits of charged particles are larger than those of neutral particles.

Preprints (www.preprints.org) | NOT PEER-REVIEWED | Posted: 1 June 2023 doi:10.20944/preprints202306.0087.v1

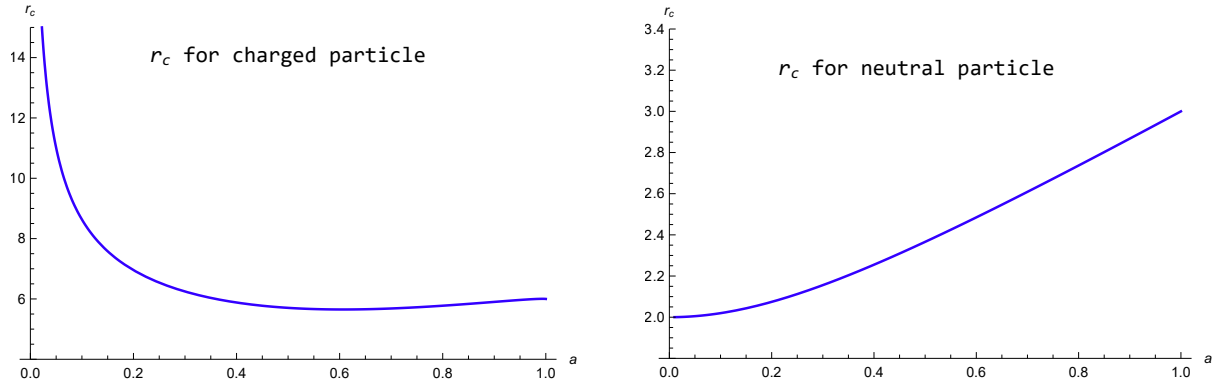

FIG. 9: The graph shows the circular orbits as a function of the interpolation parameter a for charged and neutral particles ($M = 1, q = -0.8$). The r_c increases with a decrease in the parameter a for a charged particle, contrary to a neutral particle.

VI. FORCE ON PARTICLES AND THE LYAPUNOV EXPONENT IN SEBH

The effective force acting on particle describes the motion of information, i.e., whether it is attracted toward the BH or moving away from it. We can compute the effective force on a photon and a massive particle by [44]. For photons

$$F = -\frac{1}{2}\frac{dV_{eff}(r)}{dr}, \tag{64}$$

$$F = \frac{\ell^2 r - 3M\ell^2}{2r^4} + \frac{M^2(1-a^2)\ell^2}{r^5}. \tag{65}$$

Because $(0 < a \leq 1)$, the effective force on a photon is always repulsive, as shown by equation (65). For massive particles

$$F = \frac{-3M\ell^2 + \ell^2 r - Mr^2}{2r^4} + \frac{M^2(1-a^2)(\ell^2 + r^2)}{r^5}, \tag{66}$$

we see that, the force (66) is also repulsive without any conditions. Figure 10 depicts a graphical analysis of effective force as a function of r for various values of the parameter a to study the behavior of force against the interpolation parameter a. The figure shows that the effective force is more attractive at large values of a than at small values of a, and the force does not change much as the radial distance increases. Effective forces on photons and massive particles generally point away from the BH.

On the other hand, the Lyapunov exponent gives a measure of the average rate of convergence or divergence of the nearby trajectories in the phase space. Positive Lyapunov

Preprints (www.preprints.org) | NOT PEER-REVIEWED | Posted: 1 June 2023 doi:10.20944/preprints202306.0087.v1

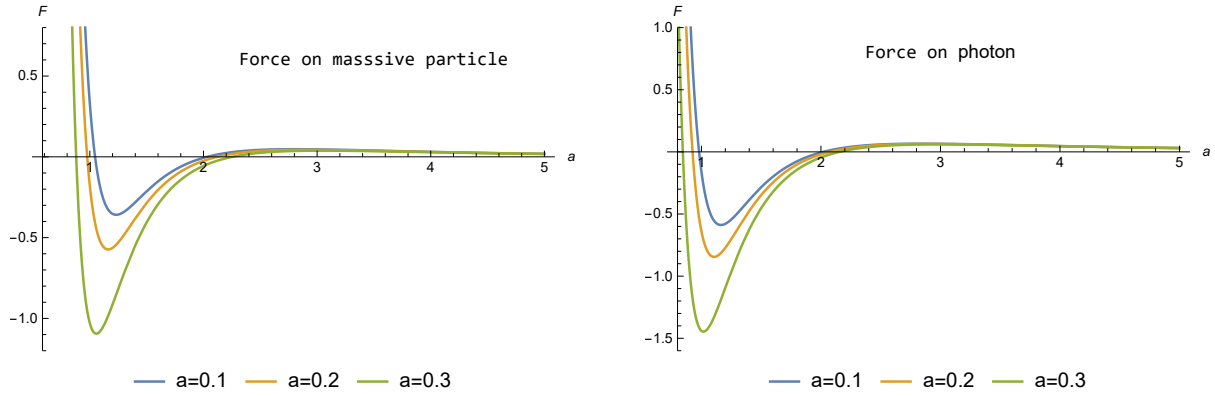

FIG. 10: Effective force versus the interpolation parameter a. The graphs illustrate the behavior of an effective force for massive particles and photons. (M = 1 and $\ell = 4$.).

exponent implies divergence between two nearby paths, meaning the paths are highly sensitive to initial conditions. In contrast, a negative Lyapunov exponent indicates contraction between two nearby geodesics. So we can check the stability of null geodesics by calculating the Lyapunov exponent [45]

$$\lambda = \sqrt{\frac{-V''_{eff}\left(r_c\right)}{2\dot{t}\left(r_c\right)^2}}$$

$$= \sqrt{\frac{-10M^4\left(1-a^2\right)^2}{r_c^6} + \frac{32M^3\left(1-a^2\right)}{r_c^5} - \frac{M^2\left(37-13a^2\right)}{r_c^4} + \frac{18M}{r_c^3} - \frac{3}{r_c^2}} \tag{67}$$

We have plotted Lyapunov exponent λ as a function of interpolation parameter a in Fig. 11. It shows that the greater the a-parameter, the larger λ will be. We conclude that the instability of null circular orbits is greater for SEBH than SBH. To find the critical exponent for instability of the orbits we use [44]

$$\gamma = \frac{T_\lambda}{T_\tau}, \tag{68}$$

where, T_λ is the instability time scale given by $T_\lambda = 1/\lambda$ and T_τ is the time period for a circular orbit which can be obtained from Eq. (10).

VII. CONCLUSION

In this paper, we investigate the motion of neutral and charged particles in a spacetime that represents a mass M coupled to an external EM field. To investigate the paths of the particles, we did a comprehensive study of null and timelike geodesics around the SEBH. The

Preprints (www.preprints.org) | NOT PEER-REVIEWED | Posted: 1 June 2023 doi:10.20944/preprints202306.0087.v1

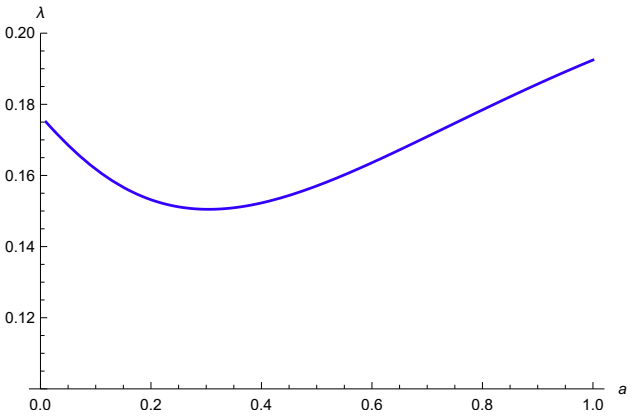

FIG. 11: The Lyapunov exponent as a function of interpolation parameter a for M = 1 and $\ell = 2$.

equations for the geodesics were solved in terms of Jacobi-elliptic integrals for various values of energy and angular momentum of the photons and massive particles. In null geodesics, we discovered two types of unstable circular orbits. The first type of circular orbit begins at infinity and approaches the BH, while the second type of orbit begins above the event horizon and ends below the inner horizon. In the case of timelike geodesics, the effective potential of a massive test particle is studied in detail. We have different particle motion scenarios that correspond to different energy levels. We have stable and unstable circular orbits, bound and unbound orbits, and fly-by orbits, for example.

When the particle has a charge, however, the Lagrangian has an additional term that is expressed in terms of the charge q. As a result, the sign of q becomes significant. When analyzing circular motion, the effect of the charged sign is distinguished when the charge is positive, demonstrating that the behavior of the charged particle is unphysical due to the collision of forces, the attractive gravitational force and the repulsive electric force. However, if the sign is negative, the effect of the sign is negligible because both forces are attractive. In addition, the radius of ISCO for a charged particle is obtained, and it is demonstrated that as the interpolation parameter increases, the radius decreases, in contrast to the case of a neutral particle. The effective force acting on photons and massive particles has been studied. It is observed that the effective force is always repulsive without condition, and it is more attractive when the interpolation parameter a is larger. In addition, we discussed the instability of circular photon orbits using the Lyapunov exponent. According to our results, Lyapunov exponent increases with a higher value of the interpolation parameter,

and the Null circular-orbit instability of Schwarzschild with EM field is greater than bare Schwarzschild BH.

In conclusion, some of the most important results are summarized below. Geodesics in SBH and SEBH differ mainly because g(u) is quartic in the latter and cubic in the former. Therefore, in SEBH, the orbits of the second kind do not end into a singularity like in SBH, they end at a limited distance below r_{in}. Further, the radius of ISCO for a charged particle in SEBH depends on three parameters q, M and a and is larger than that of SBH. Finally, as an extension of this work, we will study the bending angle of light around the SEBH and investigate the strong gravitational lensing. In this study, it would be interesting to investigate the effects of the external electromagnetic field and compare those results with those of SBH.

Data Availability and Ethical Statement

No data availability in this manuscript. This is an original work that has not been published anywhere else in any form or language. There is no conflict of interest.

References

[1] M. Halilsoy and A. Al-Badawi, *Nuovo Cimento B* **113**, 761 (1998).

[2] M. Halilsoy, *Gen. Relativ. Gravit.* **25** 275 (1993).

[3] M. Halilsoy and A. Al-Badawi *Class. Quantum Grav.* **12** 3013 (1995).

[4] I. Robinson *Bull. Acad. Pol. Sci.* **7** 351 (1959).

[5] B. Bertotti *Phys. Rev.* **116** 1331 (1959).

[6] Y. Hagihara *Jpn. J. Astron. Geophys.* **8** 67 (1931).

[7] F. Gackstatter *Ann. Phys.* **495** 352 (1983).

[8] S. Grunau and V. Kagramanova *Phys. Rev. D* **83** 044009 (2011).

[9] D. C. Wilkins *Phys. Rev. D* **5** 814 (1972).

[10] S. Chandrasekhar, *The Mathematical Theory of Black Holes (Clarendon Press* London, (1983).

[11] V. Kagramanova, J. Kunz, E. Hackmann, and C. L¨ammerzahl *Phys. Rev., D* **81** 124044 (2010).

[12] E. Hackmann and H. Xu *Phys. Rev. D* **87** 124030 (2013).

[13] P. Pradhan *Class. Quantum Grav.* **32** 165001 (2015).

[14] G. V. Kraniotis and S. B. Whitehouse *Class. Quantum Grav.* **20** 4817 (2003).

[15] N. Cruz, M. Olivares and J. R. Villanueva *Class. Quantum Grav.* **22** 1167 (2005).

[16] E. Hackmann and C. Lammerzahl *Phys. Rev. D* **78** 024035 (2008).

[17] A. Abdujabbarov and B. Ahmedov *Phys. Rev. D* **81** 044022 (2010).

[18] V. Kagramanova and S. Reimers *Phys. Rev D* **86** 084029 (2011).

[19] E. Hackmann and C. Lammerzah *Phys. Rev. Lett.* **100** 171101 (2008).

[20] S. Grunau and V. Kagramanova and J. Kunz and C. Lammerzah *Phys. Rev.D* **86** 104002 (2012).

[21] S. Grunau and V. Kagramanova and J. Kunz *Phys. Rev. D* **87** 044054 (2013).

[22] Geneviève Vachon, Robert Vanderwee and Valerio Faraonic *Eur. Phys. J. C* **81** 820 (2021).

[23] Marco Cariglia1, Tsuyoshi Houri, Pavel Krtouš and David Kubizňák *Eur. Phys. J. C* **78** 661 (2018).

[24] M. Kerachian *Phys. Rev. D* **101** 083536 (2020).

[25] V. Faraoni, F. Atieh *Phys. Rev. D* **102** 044020 (2020).

[26] E. Elizalde, G. G. L. Nashed, S. Nojiri and S. D. Odintsov *Eur. Phys. J. C* **80** 109 (2020).

[27] R. P. Eatough, H. Falcke, R. Karuppusamy, K. J. Lee, D. J. Champion, E. F. Keane,G. Desvignes, D. H. F. M. Schnitzeler, L. G. Spitler, M. Kramer, B. Klein, C. Bassa, G. C. Bower, A. Brunthaler, I. Cognard, A. T. Deller, P. B. Demorest, P. C. C. Freire,A. Kraus, A. G. Lyne, A. Noutsos, B. Stappers, and N. Wex *Nature* **501** 391 (2013) arXiv:1308.3147.

[28] N. S. Kardashev *Mon. Not. R. Astron. Soc.* **276** 515 (1995).

[29] A. Bakhan'kov *Phy. Lett. A* **139** 125 (1989).

[30] V. Karas and D. Vokrouhlicky *Class. Quant. Grav.* **7** 391 (1990).

[31] R. Brito, V. Cardoso, and P. Pani *Phys. Rev. D* **89** 104045 (2014). arXiv:1405.2098.

[32] V. Karas and D. Vokrouhlick *Gen. Rel. Grav.* **24** 729 (1992).

[33] M. Santoprete and G. Cicogna *Gen. Rel. Grav.* **34** 1107 (2002).

[34] G. Preti *Class. Quant. Grav.* **21** 3433 (2004).

[35] A. Aliev and N. Ozdemir *Mon. Not. Roy. Astron. Soc.* **336** 241 (2002).

[36] A. Al-Badawi, M. Q. Owaidat and S. Tarawneh *Int. J. Mod. Phys. D* **26** 1750169 (2017).

[37] A. Ovgun *Int. J. Theor. Phys.* **55** 2919 (2016).

[38] A. Ovgun, I. Sakalli, J. Saavedra *Chinese Physics C, No. 10* **42** 105102 (2018).

 doi:10.20944/preprints202306.0087.v1

[39] D. Pugliese, H. Quevedo, R. Ruffini *Phys. Rev. D* **83** 2 (2011).

[40] D. Pugliese, H. Quevedo, R. Ruffini *Phys. Rev. D* **84** 044030 (2011). arXiv:1105.2959.

[41] D. Pugliese, H. Quevedo, R. Ruffini *Eur. Phys. J.C* **71** 1638 (2011).

[42] 1. D. Pugliese,H.Quevedo, R. Ruffini *Eur. Phys. J. C* **77** 206 (2017) .arXiv:1304.2940.

[43] E. T. Newman and R. Penrose *J. Math. Phys.* **3** 566 (1962), Erratum 4 (1963) 998.

[44] S. Fernando *Gen. Relativ. Gravit.* **44** 1857 (2012).

[45] V. Cardoso, A. S. Miranda, E. Berti, H. Witeck, and V. T. Zanchin *Phys. Rev. D* **79** 064016 (2009).